Simulations of Discrete Quantum Systems in Continuous Euclidean Time

B. B. Beard and U.-J. Wiese

Center for Theoretical Physics, Laboratory for Nuclear Science, and Department of Physics,
Massachusetts Institute of Technology, Cambridge, Massachusetts 02139
(Received 27 February 1996)

We propose a new method to study path integrals for discrete quantum systems in which we work directly in the Euclidean time continuum. The method is of general interest. Here it is applied to the Heisenberg quantum antiferromagnet using a continuous-time version of a loop cluster algorithm. This algorithm is exploited to confirm the predictions of chiral perturbation theory in the extreme low temperature regime, down to $T = 0.01J$. A fit of the low-energy parameters of chiral perturbation theory gives excellent agreement with previous results and with experiments. [S0031-9007(96)01873-X]

The path integral for a general quantum system is usually implemented in discrete time. Farhi and Gutmann showed how to build a path integral in continuous time for quantum systems in a *discrete basis* [1]. The paths consist of segments for which the system is in a basis state for a finite time, with sporadic discrete transitions between basis states. This insight can be applied, for example, to quantum spin systems, lattice fermions, and lattice gauge theories with a compact gauge group. The work described here is the first application of this technique to a problem of practical interest.

In the continuous-time formulation a path is characterized by transition times and information about which states are connected at the transitions. This picture allows the path integral to be sampled numerically without having to store information about individual time slices. In the discrete-time approximation one must always exercise care in extrapolating the results to the time-continuum limit. The approach advocated here, where we operate directly in this limit, completely eliminates the most severe systematic error in these calculations.

As an example we consider quantum spin systems. Conventional approaches to handling these systems rely on a discrete-time formalism. Consider the Hamiltonian for the quantum antiferromagnetic Heisenberg model (AFHM)

$$H = J \sum_{x,\mu} \vec{S}_x \cdot \vec{S}_{x+\hat{\mu}}, \qquad (1)$$

where $\vec{S}_x = \frac{1}{2}\vec{\sigma}_x$ is a spin $\frac{1}{2}$ operator associated with the site x of a d-dimensional hypercubic lattice. The interaction is between nearest neighbors; $\hat{\mu}$ is the unit vector in the μ direction. For an antiferromagnet the coupling constant J is positive. Since this Hamiltonian comprises noncommuting terms, the explicit evaluation of the associated partition function is problematical. Suzuki is credited with showing how the Trotter formula can be applied to segregate these noncommuting terms into separate time slices, with the approximation becoming exact in the continuum limit [2]. For example, the Hamiltonian of a 1D quantum spin chain can be decomposed into two terms, $H = H_1 + H_2$, each of which comprises only commuting terms

$$H_1 = J \sum_{x=2m} \vec{S}_x \cdot \vec{S}_{x+\hat{1}}, \qquad H_2 = J \sum_{x=2m+1} \vec{S}_x \cdot \vec{S}_{x+\hat{1}}. \qquad (2)$$

Then for the partition function one writes

$$Z = \text{Tr} \exp(-\beta H)$$
$$= \lim_{N \to \infty} \text{Tr}[\exp(-\varepsilon\beta H_1)\exp(-\varepsilon\beta H_2)]^N, \qquad (3)$$

where $\beta = 1/T$ is the inverse temperature and $\varepsilon\beta = \beta/N$ is the lattice spacing in Euclidean time. Inserting complete sets of eigenstates $|\pm\frac{1}{2}\rangle$ of S_x^3 between the factors $\exp(-\varepsilon\beta H_i)$ one converts the partition function into a $(d+1)$-dimensional path integral of Ising-like variables

$$Z = \prod_{x,t} \sum_{s(x,t)=\pm 1/2} \exp(-S). \qquad (4)$$

The action is a sum of plaquette couplings in a "checkerboard" pattern

$$S = \sum_{x=2m,t=2p} S[s(x,t), s(x+\hat{1}), s(x,t+1), s(x+\hat{1}, t+1)]$$

$$+ \sum_{x=2m+1,t=2p+1} S[s(x,t), s(x+\hat{1}), s(x,t+1), s(x+\hat{1}, t+1)],$$

and the plaquette Boltzmann factors are given by a 4×4 transfer matrix

$$\exp(-S[s_1, s_2, s_3, s_4])$$
$$= \langle s_1 s_2 | \exp(-\varepsilon \beta J \vec{S}_x \cdot \vec{S}_{x+\hat{\mu}}) | s_3 s_4 \rangle.$$

For the spin $\frac{1}{2}$ AFHM, only 6 of the 16 elements of the transfer matrix are nonzero, namely, those that leave the three-component of spin unchanged.

The 2D Heisenberg model is of interest because it describes the undoped precursor insulators of high temperature superconductors. It has been studied with various Monte Carlo techniques [3], including a very efficient loop cluster algorithm [4,5]. The cluster algorithm has led to a very precise determination of the low energy parameters of the Heisenberg model [5], consistent with the chiral perturbation theory treatment of Hasenfratz and Niedermayer [6]. These parameters are consistent with experimental data on precursor insulators of high temperature superconductors [7,8].

The loop cluster algorithm in two spatial dimensions and discrete time is implemented on a lattice with $(L/a)^2$ spatial points and $4N$ time slices, so the total number of sites is $N_l = 4N(L/a)^2$. Each lattice site is assigned a spin with a $\pm\frac{1}{2}$ spin state. Periodic boundary conditions are applied in space and time. As described above, an action is defined for each of the 2^{N_l} lattice configurations by working with plaquettes that span nearest neighbors in space and time, in a pattern that resembles a checkerboard in $(2 + 1)$-dimensional space. The basic idea is to build closed loops of spin sites and then flip all the spins on the loop. The rules for building loops are designed to provide ergodicity and detailed balance [4].

To build a loop, it is necessary to decide how it will flow through each of the different types of plaquettes that have finite action. Table I displays the three types of finite-action plaquettes for the spin $\frac{1}{2}$ AFHM, together with flow patterns that have been determined to provide detailed balance.

The first pattern in Table I, with "like" spins on all four corners of the plaquette, forces the flow to proceed in the time direction. The second pattern, with alternating spins, forces the flow to move to the adjacent spin site at constant time. The third pattern, with "unlike" spins at adjacent spin sites, is probabilistic. The first time a loop encounters such a plaquette, the flow is sent in the time direction with probability p. If the flow happens to revisit the plaquette, it is forced to conform to the flow direction that was chosen at the initial visit. These three types of plaquettes are referred to as "forced continuation," "forced transition," and "optional decay," respectively.

The loop is constructed piecewise until it closes. The loop-building rules ensure that the loops always close.

Figure 1 shows a typical situation in the building of a loop in $(1 + 1)$ dimensions with discrete time. Here we show the neighborhood of site i, for a number of time slices. Filled circles indicate spin up sites; open circles, spin down. The hatched rectangles are the plaquettes

TABLE I. Summary of plaquette flow rules. Solid circles and lines indicate spin up sites; open circles and dotted lines are spin down. The time direction is horizontal. Flow rules for inverse plaquettes are analogous.

	Discrete time	Continuous time
Forced continuation		
Forced transition		
Optional decay, $p = 2/[1 + \exp(\epsilon\beta J)]$ and $\lambda = J/2$		

resulting from the Trotter-Suzuki decomposition. A loop is shown entering this diagram at t_1. It is forced to proceed forward in time for two plaquettes, then encounters a series of optional decay plaquettes. It is shown succumbing to the temptation to move to site $i - 1$ at time t_7. Note that if it had reached time t_{10}, it would have been forced to move to site $i + 1$.

To go to the continuum limit of the cluster-building algorithm, first visualize a given lattice configuration with successively finer granularity in time. The time variation of the spin state at a given site is seen to comprise segments for which the system is in a state for a finite time, with sporadic discrete transitions between states. We build loops in the same way: Loop movement from one spin site to a neighbor is sporadic and most of the (now infinitesimal) plaquettes are continuations in time.

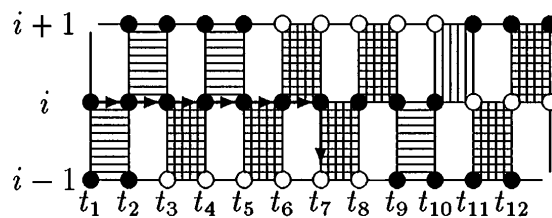The essential difference between the discrete-time and continuous-time implementation is that the former

FIG. 1. Typical situation in the building of a path in discrete time and one spatial dimension. Time is in the horizontal direction; the immediate neighborhood of spin site i is depicted in the vertical direction. Solid circles denote spin-up sites; open circles denote spin down.

requires us to store spin state information for each of the points of the space-time lattice, while the latter requires us only to store the transition times for each spin site (plus an extra bit to record the state at $t = 0$). As discussed below, the time evolution of the path is also handled differently; instead of a point-by-point crawl through the lattice, we race through time because we know the decay times are exponentially distributed.

The last column of Table I shows the continuum-time flow rules. Solid lines represent continuously spin-up states; dotted lines, spin down. The flow rule for the forced continuation plaquettes has, in the continuum limit, become a rule that the flow cannot move to a neighbor that is in the same spin state. It is the forced transition plaquettes which represent the discontinuous change in spin state; we call the resulting jumps "bonds" because the changes in state at a given site are always accompanied by complementary changes in a neighbor. The continuum limit of the flow rule for the forced transition plaquettes is the rule that, if the flow reaches a bond, it must follow it to the neighbor and reverse direction.

The rule for the optional decay plaquettes, which is probabilistic, becomes a rule that the flow will jump to a neighbor in an opposite state with a fixed probability per unit time. The resulting exponential distribution of segment lengths is identical to the familiar distribution of the lifetime of a radioactive nucleus. The decay constant is simply $\lambda = \lim_{\epsilon \to 0}(1 - p)/\epsilon\beta = J/2$.

Figure 2 shows a typical situation in the building of a loop in $(1 + 1)$ dimensions with continuous time. Again we show the neighborhood of site i. Solid lines indicate spin-up sites; dotted lines, spin down. A loop is shown entering the diagram at t_1. The probability per unit time that it will move to a neighboring site is proportional to the number of neighbors that are of opposite spin. The total decay constant λ is shown varying with time in the graph in Fig. 2. For example, between t_2 and t_3 there are no available "decay channels" and the flow is forced to move forward in time in that interval. In the situation
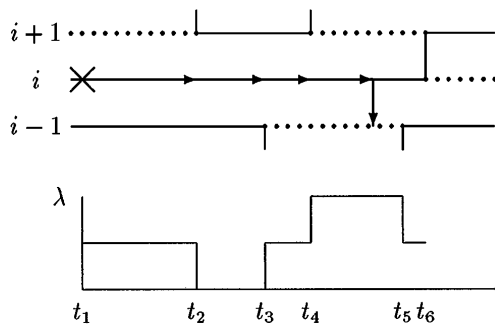

FIG. 2. Typical situation in the building of a path in continuous time and one spatial dimension. Solid lines denote spin-up sites in continuous time; dotted lines, spin down. λ is the probability per unit time that the path will jump to an adjacent site, and is proportional to the number of neighboring sites that have opposite spin.

shown here, the flow survives up to some point between times t_4 and t_5, when it decays to site $i - 1$. Note that if the flow had reached time t_6, it would have been forced to traverse the bond and move to site $i + 1$. Path building proceeds in this way until the loop closes.

A significant advantage of the loop cluster algorithm is that it allows for the implementation of improved estimators. Reference [9] discusses the development of improved estimators for cluster algorithms. We found that the improved estimators for susceptibility, staggered susceptibility, and internal energy density all have easily determined continuum limits.

Results of the continuous-time algorithm [10] were verified against exact solutions for the two- and four-spin cases, as well as for previous results for the 1D and 2D Heisenberg antiferromagnets and the 1D Heisenberg ferromagnet [5,11]. In all cases the results were consistent with previously established results.

The continuum-time method completely eliminates the most severe systematic error in this type of calculation. It also obviates the need to conduct the several runs of successively finer time granularity needed for extrapolation to the continuum limit, thus eliminating a costly dimension in the simulation procedure.

In the ground state of the 2D AFHM the staggered magnetization develops an expectation value, and hence the O(3) spin rotational symmetry gets spontaneously broken down to O(2). The low energy excitations of the system are spin waves (so-called magnons) which are the Goldstone bosons of the spontaneously broken O(3) symmetry. Chiral perturbation theory (CPT) provides a powerful set of tools for analyzing such systems. CPT starts with the most general effective local action which respects all the symmetries of the system. In this case CPT predicts magnon dynamics at low temperatures with three parameters as unknown constants: the staggered magnetization $\mathcal{M}_s$, the spin wave velocity c, and the spin stiffness ρ_s. The predictions of CPT at extremely low temperatures are investigated using a range of square volumes with side length $L = 6, 8, \ldots, 20$ and a range of inverse temperatures $\beta J = 1, 2, 5, 10, 20, 30, 40, 50, 80, 100$. Note that the very small temperatures $T \approx 0.01J$ are inaccessible to the discrete-time code, largely due to storage limitations.

Several of the key predictions of CPT were directly verified with this code. In particular, the energy spectrum is that of an O(3) rotor, with energy levels characterized by an integer spin j, having degeneracy $2j + 1$ and energy proportional to $j(j + 1)$. Finite volume effects are computed as expansions in $\hbar c/\rho_s L$. The energy spectrum is computed in Ref. [6] to be

$$E_j = j(j + 1)\frac{(\hbar c)^2}{2\rho_s L^2}\left[1 - \frac{\hbar c}{\rho_s L}\frac{3.900265}{4\pi} + O(L^{-2})\right].$$

The leading term of the uniform susceptibility is

$$\chi_u \xrightarrow[T \to 0]{} \frac{6}{L^2 T} \exp\left(-\frac{(\hbar c)^2}{\rho_s L^2 T}\right), \qquad (5)$$

TABLE II.   Comparison of fitted parameters.

	Ref. [5]	Current
Spin stiffness ρ_s	0.186(4)	0.185(2)
Spin wave velocity $\hbar c$	1.68(1)	1.68(1)
Staggered magnetization $\mathcal{M}_s$	0.3074(4)	0.3083(2)
Quadratic coefficient: energy	$\cdots$	0.068(1)
Quadratic coefficient: χ_s	$\cdots$	0.338(7)

and the staggered susceptibility goes to the temperature-independent form

$$\chi_s \underset{T\to 0}{\longrightarrow} \frac{2\mathcal{M}_s^2 \rho_s}{(\hbar c)^2} L^4 \left[1 + 3 \frac{\hbar c}{\rho_s L} \frac{3.900265}{4\pi} + O(L^{-2}) \right].$$

(6)

These functional forms in the large β limit, including both volume and temperature dependence, were verified for uniform and staggered susceptibility.

An independent fit for the CPT parameters $\mathcal{M}_s$, $\hbar c$, and ρ_s gives excellent agreement with the results of [5], as shown in Table II. This fit required that the partition function of the O(3) rotor be included in its entirety, instead of including just the leading term, as the limiting forms in Eqs. (5) and (6) employ. In addition, only inverse temperatures $\beta J \geq 10$ were used in the fit, since the rotor description is valid only for very small temperatures. In order to reproduce the accuracy of the fit in Ref. [5], it was necessary to find fitted values for the coefficients of the quadratic terms in the expressions for energy and staggered susceptibility, that is, the coefficients of the terms $(\hbar c/\rho_s L)^2$ in the expressions above. Note that the agreement between the current work and Ref. [5] is particularly remarkable because they are based on different volume-temperature regimes. Reference [5] was concerned with the "cubical" regime $TL/\hbar c \cong 1$, while the current study focuses on the "cylindrical" regime $TL/\hbar c \ll 1$. The five parameter values in Table II resulted in a goodness-of-fit $\chi^2/\text{d.o.f.} = 1.5$. Figures 3(a) and 3(b) show the fit for uniform and staggered susceptibility, respectively. Solid lines represent the fitted CPT result. Circles and error bars are displayed at each simulation point. The fit is very good for $\beta J \geq 10$.

In conclusion, we find that the continuous-time formulation discussed here provides a superior method for evaluating path integrals that arise in the study of discrete quantum systems. The continuum-time implementation of path integrals can be applied to a wide variety of problems. For example, it can be applied to a loop cluster algorithm that has been constructed for lattice fermions [12]. It works in principle for any quantum system in a discrete basis, even if a cluster algorithm may not be available. For example, for a lattice gauge theory with a compact gauge group one can work in the discrete basis of representations.

We thank P. Grassberger for asking a question that led to this project. We also thank E. Farhi and S. Gutmann
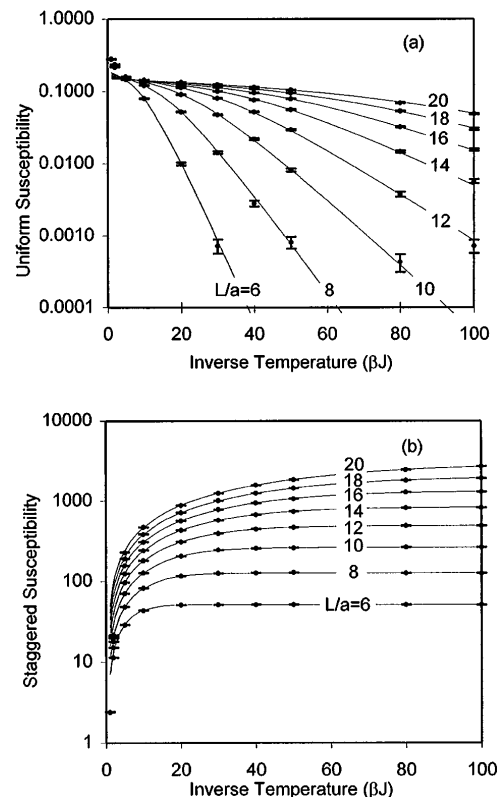

FIG. 3.   (a) Uniform susceptibility and (b) staggered susceptibility versus inverse temperature for various volumes. Solid lines are predictions from chiral perturbation theory with fitted parameters; circles with error bars are lattice simulations with continuous time. The fit is very good for $\beta J \geq 10$.

[1] E. Farhi and S. Gutmann, Ann. Phys. (N.Y.) **213**, 182 (1992).
[2] M. Suzuki, Prog. Theor. Phys. **56**, 1454 (1976).
[3] M. S. Makivić and H.-Q. Ding, Phys. Rev. B **43**, 3562 (1991).
[4] H. G. Evertz, G. Lana, and M. Marcu, Phys. Rev. Lett. **70**, 875 (1993).
[5] U.-J. Wiese and H.-P. Ying, Z. Phys. B **93**, 147 (1994).
[6] P. Hasenfratz and F. Niedermayer, Z. Phys. B **92**, 91 (1993).
[7] G. Shirane et al., Phys. Rev. Lett. **59**, 1613 (1987).
[8] M. Greven et al., Z. Phys. B **96**, 465 (1995).
[9] U. Wolff, Phys. Rev. Lett. **62**, 361 (1989); U. Wolff, Nucl. Phys. **B334**, 581 (1990).
[10] This code will be made available via the World Wide Web. Check http://ctpa02.mit.edu/~bbbeard/ for details.
[11] U.-J. Wiese and H.-P. Ying, Phys. Lett. A **168**, 143 (1992).
[12] U.-J. Wiese, Phys. Lett. B **311**, 235 (1993).